THE UNIVERSITY of EDINBURGH

Edinburgh Research Explorer

Assessing the impact of different penalty factors of the Bayesian reconstruction algorithm Q.Clear on in vivo low count kinetic analysis of [11C]PHNO brain PET-MR studies

Citation for published version:
Ribeiro, D, Hallett, W, Howes, O, McCutcheon, R, Nour, MM & Tavares, AAS 2022, 'Assessing the impact of different penalty factors of the Bayesian reconstruction algorithm Q.Clear on in vivo low count kinetic analysis of [11C]PHNO brain PET-MR studies', *EJNMMI research*. https://doi.org/10.1186/s13550-022-00883-1

Digital Object Identifier (DOI):
10.1186/s13550-022-00883-1

Link:
Link to publication record in Edinburgh Research Explorer

Document Version:
Peer reviewed version

Published In:
EJNMMI research

General rights
Copyright for the publications made accessible via the Edinburgh Research Explorer is retained by the author(s) and / or other copyright owners and it is a condition of accessing these publications that users recognise and abide by the legal requirements associated with these rights.

Take down policy
The University of Edinburgh has made every reasonable effort to ensure that Edinburgh Research Explorer content complies with UK legislation. If you believe that the public display of this file breaches copyright please contact openaccess@ed.ac.uk providing details, and we will remove access to the work immediately and investigate your claim.

OPEN ACCESS

Download date: 17. May. 2022

Assessing the impact of different penalty factors of the Bayesian reconstruction algorithm Q.Clear on *in vivo* low count kinetic analysis of [^{11}C]PHNO brain PET-MR studies

Daniela Ribeiro[1,2], William Hallett[1], Oliver Howes[3,4,5], Robert McCutcheon[3,4,5], Matthew M. Nour[3,6,7], Adriana A. S. Tavares[2]

[1]Invicro, Centre for Imaging Sciences, Hammersmith Hospital, London, UNITED KINGDOM

[2]Edinburgh Imaging, The University of Edinburgh, Edinburgh, UNITED KINGDOM

[3]Institute of Psychiatry, Psychology & Neuroscience, King's College London, London, UNITED KINGDOM

[4]Medical Research Council London, Institute of Medical Sciences, London, UNITED KINGDOM

[5]Institute of Clinical Sciences, Faculty of Medicine, Imperial College London, London, UNITED KINGDOM

[6]Max Planck Centre for Computational Psychiatry and Ageing Research, Institute of Neurology, University College London, London, UNITED KINGDOM

[7]Wellcome Centre for Human Neuroimaging, Institute of Neurology, University College London, London, UNITED KINGDOM

Corresponding Author:

Name: Daniela Ribeiro

Address: Invicro, Burlington Danes Building, Hammersmith Hospital, Imperial College London, Du Cane Road, London W12 0NN

Phone: 07475946297

Email: Daniela.Ribeiro@invicro.co.uk

Word count: 4153

Abstract

Introduction: Q.Clear is a Bayesian penalised likelihood (BPL) reconstruction algorithm available on General Electric (GE) Positron Emission Tomography (PET)-Computed Tomography (CT) and PET-Magnetic Resonance (MR) scanners. This algorithm is regulated by a β value which acts as a noise penalisation factor and yields improvements in signal to noise ratio (SNR) in clinical scans, and in contrast recovery and spatial resolution in phantom studies. However, its performance in human brain imaging studies remains to be evaluated in depth. This pilot study aims to investigate the impact of Q.Clear reconstruction methods using different β value versus ordered subset expectation maximization (OSEM) on brain kinetic modelling analysis of low count brain images acquired in the PET-MR.

Methods: Six [^{11}C]PHNO PET-MR brain datasets were reconstructed with Q.Clear with β100 to 1000 (in increments of 100) and OSEM. The binding potential relative to non-displaceable volume (BP_{ND}) were obtained for the Substantia Nigra (SN), Striatum (St), Globus Pallidus (GP), Thalamus (Th), Caudate (Cd) and Putamen (Pt), using the MIAKAT ™ software. Intraclass correlation coefficients (ICC), repeatability coefficients (RC), coefficients of variation (CV) and bias from Bland-Altman plots were reported. Statistical analysis was conducted using a 2-way ANOVA model with correction for multiple comparisons.

Results: When comparing a standard OSEM reconstruction of 6 iterations/16 subsets and 5mm filter with Q.Clear with different β values under low counts, the bias and RC were lower for Q.Clear with β100 for the SN (RC=2.17), Th (RC=0.08) and GP (RC = 0.22) and with β200 for the St (RC=0.14), Cd (RC=0.18)and Pt (RC=0.10). The p-values in the 2-way ANOVA model corroborate these findings. ICC values obtained for Th, St, GP, Pt and Cd demonstrate good reliability (0.87, 0.99, 0.96, 0.99 and 0.96, respectively). For the SN, ICC values demonstrate poor reliability (0.43).

Conclusion: BP_{ND} results obtained from quantitative low count brain PET studies using [^{11}C]PHNO and reconstructed with Q.Clear with β<400, which is the value used for clinical [^{18}F]FDG whole-body studies, demonstrate the lowest bias versus the typical iterative reconstruction method OSEM.

Keywords: PET-MR, [^{11}C]PHNO, reconstruction, Bayesian, neuroimaging

1. Introduction

Positron Emission Tomography (PET) is an imaging technique that allows for non-invasive quantitative measurement of biological processes *in vivo*. Filtered Back Projection (FBP) has been used as the preferred reconstruction method in dynamic quantitative brain PET imaging research due its linearity, robustness and reliable results however Ordered Subset Expectation Maximisation (OSEM) is often used for semi-quantitative clinical whole-body and brain imaging due to its ability to provide better image quality [1]. FBP is not available in recently developed scanners, including the General Electric (GE) Signa PET- Magnetic Resonance (MR) scanners and therefore other alternatives have been devised. Current reconstruction algorithms such as OSEM and Block Sequential Regularised Expectation Maximisation (BSREM) are considered iterative reconstruction algorithms and can be used in images acquired in PET-Computed Tomography (CT) and in PET-MR scanners [2]. Previous studies [3–5] conducted in PET-CT scanners have demonstrated that OSEM presents better image quality and signal to noise ratio than FBP, therefore making it a suitable alternative to be used in clinical brain studies acquired in the PET-MR scanner. The suitability of BSREM algorithms in this setting has however not been extensively explored. Moreover, it has been shown that results obtained from OSEM reconstructions are biased in low statistics and it is unclear if BSREM algorithms perform in the same way [1].

The BSREM algorithm is a Bayesian penalised likelihood (BPL) reconstruction algorithm that uses prior knowledge as a penalty term in the iterative process. The β value (editable parameter in the algorithm) regulates the strength of the penalty term, acting as a noise penalisation factor and improves the Signal to Noise ratio (SNR). GE Healthcare has released the BSREM penalised likelihood reconstruction algorithm with the denomination of Q.Clear [6,7]. PET images can be analysed with qualitative methods, which are based on visual assessments, and semi-quantitative or quantitative methods, such as standard uptake values or volumetric measurements, respectively [8]. The literature regarding the use of Q.Clear as a reconstruction algorithm for quantification is limited, with some manuscripts investigating the effect of the algorithm in phantom images [7,9,10]. Most of the available literature is primarily focused on fluorinated tracers, with some publications investigating the effect of the algorithm in semi-quantification of whole-body scans and/or small structures imaging [11–14]. Furthermore, there is limited knowledge on the quantitative accuracy of Q.Clear when reconstructing brain PET-MR images with low counts and high noise.

[^{11}C]PHNO is a PET radiotracer that binds to both D2 and D3 dopamine receptors which are part of the D2-like dopaminergic receptors (DARs) family [15,16]. Unlike antagonist radiopharmaceuticals, agonist radiotracers such as [^{11}C]PHNO have the potential to produce pharmacologic effects [17,18]. In practice, a compromise between mass and activity must be reached before the scan, in order to avoid side effects, and it is sometimes necessary to administer an activity much lower than the target activity [18]. The restricted injected dose limits may result in noisy imaging data with low counts. Moreover, for studies that require multiple scans, for example for longitudinal follow-up or to investigate the effects of drug challenges [19], it is necessary to limit the injected dose to ensure the total radiation dose remains within an acceptable range for research. In these circumstances it is particularly important to use a reconstruction algorithm that maximises the SNR.

Image reconstruction algorithms may have an impact on measured binding potential relative to non-displaceable volume measurements (BP_{ND}) calculated when using a simplified reference tissue model (SRTM), although this has not been fully assessed with the latest reconstruction methods, such as Q.Clear [20]. Hence, we aim to investigate the impact of Q.Clear reconstruction methods on brain kinetic modelling analysis, which will provide new knowledge compared with previously conducted studies focused on characterising simplified outcome measure bias (e.g. standard uptake value (SUV)) introduced by Q.Clear reconstruction methods. The primary objective of this pilot study is to investigate the performance of Q.Clear, against the performance of the established OSEM algorithm, in low activity [^{11}C]PHNO PET brain images acquired on a PET-MR system. We also investigate which Q.Clear β values provides similar quantitative results for low count brain scans, to those observed with a OSEM 6 iteration, 16 subset and 5mm filter reconstruction (which is a routinely used clinical standard reconstruction for brain PET-MR scans, including within our department). This will provide important evidence to the field, given that previous work has been predominantly focused on the use of Q.Clear methods for reconstruction of whole-body PET data and routine non-kinetic modelling studies.

2. Materials and Methods

2.1 [^{11}C]PHNO PET-MR human data acquisition and reconstruction

The original study adhered to the principles outlined in the National Health Service (NHS) Research Governance Framework for Health and Social Care (2nd edition), the Declaration of Helsinki and Good Clinical

Practice (GCP). It was also conducted in compliance with the Protocol, the Data Protection Act and other regulatory requirements, and Standard Operating Procedures (SOPs), as appropriate. The data that were used in this project were acquired after the participant's consent was obtained for the original study (REC reference 12/LO/1955, IRAS Project ID: 103938). Use of this data was covered in the original consent form, which stated that the data acquired could be used in future related research.

Seven *in vivo* [^{11}C]PHNO PET datasets, corresponding to seven different healthy normal participants, were reconstructed retrospectively using Q.Clear and OSEM algorithms, for this pilot study. The average age of the participants was 23 years with the female to male ratio being 3:4. The mean administered dose was 145.8±15.8 MBq (mean±SD, n=7).

An MRI-based attenuation correction (MRAC) sequence (MRI sequence with flip angle of 5 degrees, echo time (TE) 1.674ms, repetition time (TR) 4.048ms, 50x38 cm FOV with 256x128 matrix), which was obtained during scan acquisition, was used for attenuation correction of the PET data.

Typical [^{11}C]PHNO PET-MR scans were binned into the following frames 10×15s, 3×60s, 5×120s, 15×300s, with a total duration of 90 minutes and 30 seconds. The dataset was processed once with the above frames and with a reconstruction of OSEM 6iterations, 16subsets and a 5mm Gaussian filter, with time of flight (TOF) information. This was entitled "26_OSEM_6i16s5mm_normal". In order to mimic a low count acquisition, the dynamic PET-MR scans were reprocessed with a pre-frame delay thereby decreasing the time per frame by a factor of 3. Each *in vivo* dataset was reconstructed 11 times (10 TOF Q.Clear reconstructions [with β between 100 and 1000, in increments of 100], and 1 TOF OSEM reconstruction [6iterations, 16subsets and a 5mm Gaussian filter]) , with the pre-frame delay and named with the suffix "_low". Normal [^{11}C]PHNO scans present an average count level of 4.9×10^7 counts at the 15-minute frame, 1.1×10^7 counts at the 45-minute frame and 2.6×10^6 counts at the 90-minute frame. When simulating a low dose acquisition, the 15-minute frame presented an average count level of 1.5×10^7 counts, the 45-minute frame 3.3×10^6 counts and the 90-minute frame 8.3×10^5 counts. Supplementary file 1 contains a graphic of the prompt events over time, for the normal and low count datasets, for one participant. For ease of comparison, the European Association of Nuclear Medicine advises that, for static brain [^{18}F]FDG scans, 100 million events should be detected for a duration of 10 to 20 minutes [21]. The scan reconstructed with OSEM 6iterations, 16subsets and a 5mm Gaussian filter under normal counts was only used for the comparison with its counterpart under low counts, to establish the extent of the variability when using the same reconstruction parameters and different count statistics. Point Spread Function (PSF) modelling was not used for the OSEM or Q.Clear reconstructions (PSF modelling is included in Q.Clear by default) and all datasets were reconstructed using time of flight information.

2.2 Data analysis

All reconstructed [^{11}C]PHNO dynamic human brain PET scans were run through the MIAKAT™ (www.miakat.org) pipeline in order to obtain BP_{ND} results for the Substantia Nigra (SN), Striatum (St), Globus Pallidus (GP), Thalamus (Th), Caudate (Cd) and Putamen (Pt). The pipeline in MIAKAT™ follows a sequence of steps namely, Brain Extraction, Brain Tissue Segmentation, Motion Correction, Region of interest (ROI) definition, ROI tracer kinetic modelling and Parametric imaging. Motion correction and ROIs were applied to all reconstructions for the same subject. No image processing was performed prior to the datasets being run through MIAKAT™, however the outputs from the steps described above were reviewed and manually accepted by the investigator. The data analysis steps required limited interaction from the investigator and the data analysis process for all images datasets was conducted by the same investigator, hence reducing intra-operator and inter-operator variability. Since a region devoid of receptors was available, i.e. the cerebellum, it was possible to use a SRTM approach to estimate BP_{ND}, which is a product of the receptor density and affinity and provides information regarding non-specific and free radioligand concentrations [22].

Intraclass Correlation Coefficient (ICC) estimates and 95% confident intervals (CI) were calculated using SPSS statistical package version 26 (SPSS Inc, USA) based on 11 reconstruction items (TOF_OSEM_6i16s5mm_low, TOF_QClear_B100_low, TOF_QClear_B200_low, TOF_QClear_B300_low, TOF_QClear_B400_low, TOF_QClear_B500_low, TOF_QClear_B600_low, TOF_QClear_B700_low, TOF_QClear_B800_low, TOF_QClear_B900_low and TOF_QClear_B1000_low), absolute-agreement, 2-way mixed-effects model.

Bland-Altman plots were obtained with GraphPad Prism version 8.0.0 for Windows (GraphPad Software, USA). Bias and the Repeatability Coefficient (RC) between the OSEM algorithm (6iterations, 16subsets, 5mm filter reconstruction under low counts, defined as standard reconstruction for the purposes of this study) and the Q.Clear reconstructions (n=10, with differing β values), were produced using MedCalc® version 18 (MedCalc Software, Belgium), computing the standard deviation of the BP_{ND} results obtained for the healthy subjects. The 2-way ANOVA results and multi comparisons using the Bonferroni test were used to determine group differences among BP_{ND} results for the SN, St, GP, Th, Cd and Pt groups for the *in vivo* data. For this purpose, for determining the Coefficients of Variation (CV) and for graphical demonstration, GraphPad Prism version 8.0.0 for Windows (GraphPad Software, USA) was used.

3. Results

Out of the seven initial *in vivo* datasets only six were used for the statistical analysis due to one dataset presenting excessive movement that could not be corrected during image processing. It was noted that the first frames of the Q.Clear reconstructions presented spurious counts that did not correspond to the radiopharmaceutical injection, interfering with the time activity curves (TACs) and the kinetic modelling analysis. As the injection was only administered 30 seconds after the start of the acquisition, these frames were devoid of radioactivity. After removing the first three frames from the reconstructed images, the curves obtained presented the expected behaviour. An example of the model fitting for the Globus Pallidus and Cerebellum, for the same subject, when the brain images were reconstructed with Q.Clear with β100 and OSEM can be found in Fig. 1. The graphics entitled "original data" (A) and (C) demonstrate the fit obtained with all the frames included. The graphic entitled "cropped data" (B) and (D) demonstrate the fit obtained when the 3 first frames were removed hence removing the background counts that did not correspond to the radiopharmaceutical injection. Graphics (A) and (B) correspond to the data reconstructed with Q.Clear β100 whereas graphics (C) and (D) correspond to the data reconstructed with OSEM.

Example images of the [^{11}C]PHNO BP_{ND} obtained for one participant from the in vivo dataset and reconstructed with standard OSEM and Q.Clear with β100-1000 are present in Fig. 2.

For large brain regions, such as the thalamus and the striatum, the intraclass correlation coefficient analysis demonstrates that there is a good reliability, with the ICC obtained for the BP_{ND} results being 0.87 (95% CI, 0.70-0.98) for the thalamus and 0.99 (95% CI, 0.97-0.99) for the striatum.

For the Thalamus, when comparing with the standard reconstruction, the Q.Clear with β100 reconstruction presented the lowest bias (0.002) and RC (0.08). The full bias and RC results are present in Supplementary File 2. In the Striatum, the Q.Clear with β200 reconstruction presents the lowest bias (0.046) and RC (0.14), when compared to the standard reconstruction. This is demonstrated in the Bland-Altman plots of Fig. 3 and Fig. 4.

A graphic layout of the BP_{ND} obtained for the Substantia Nigra (A), Striatum (B), Globus Pallidus (C) and Thalamus (D), per reconstruction method is presented in Fig. 5.

For medium size brain regions, such as the Globus Pallidus, Putamen and Caudate the intraclass correlation coefficient analysis demonstrates that there is a good reliability (with the ICC obtained for the BP_{ND} results being 0.96 (95% CI, 0.89-0.99), 0.99 (95% CI, 0.98-0.99) and 0.96 (95% CI, 0.90-0.0.99) respectively. In the Globus Pallidus, BP_{ND} data shows that Q.Clear with β100 reconstruction presented the lowest bias (-0.087) and RC (0.22), when compared to the standard reconstruction. This is demonstrated in the Bland-Altman plots for the Globus Pallidus in the Supplementary File 3. The results for the Caudate and Putamen demonstrate a similar pattern to what was observed for the structures in graphs A, B and C in Fig. 5. When compared to the standard reconstruction, Q.Clear with β200 reconstruction presented the lowest bias and RC for both the Cd and Pt (bias of -0.041 and 0.015 and RC of 0.18 and 0.10, respectively).

For small size brain regions, namely the Substantia Nigra, the intraclass correlation coefficient analysis demonstrated poor intra-rater reliability (the ICC obtained for the BP_{ND} results for the SN was 0.43 (95% CI, 0.17-0.83). The Q.Clear reconstruction with β100 presented the lowest bias (0.979) and RC (2.17), when compared to the standard OSEM reconstruction. This is demonstrated in the Bland-Altman plots for the Substantia Nigra in the Supplementary File 4.

The BP_{ND} results in the Substantia Nigra for the OSEM 6 iterations, 16 subsets and filter of 5 mm reconstruction mimicking low counts were more dispersed (CV=45.42%) than the results for the same reconstruction with a normal number of counts (CV=28.61%) and the comparison between both datasets provided a bias of 0.469 and RC of 1.49. For all other brain regions, the dispersion was similar for both the normal counts and the reduced counts reconstructions. The full list of percentage CV is present in Supplementary File 5.

When comparing the BP_{ND} results from the standard iterative reconstruction, OSEM with 6 iterations, 16 subsets and a filter with 5mm kernel under low counts, with the Q.Clear reconstructions with different β values under low counts, for the Substantia Nigra, Globus Pallidus and Thalamus, there is no comparison that provides a p-value that is statistically significant. Conversely, the Q.Clear with a β300, 600, 800 and 900 showed statistically significant differences, when compared to OSEM with 6 iterations, 16 subsets and a filter with 5mm kernel, for the Striatum and Putamen (Fig. 6).

4. Discussion

The aim of this study was to investigate the impact of Q.Clear reconstruction methods on brain kinetic modelling analysis by evaluating the performance of Q.Clear, against the performance of OSEM in the presence of a small number of counts, in brain images acquired in a PET-MR system. To our knowledge, we are the first to investigate Q.Clear reconstruction performance for brain kinetic modelling analysis rather than simplified quantification methods like standard uptake value (SUV). We also report here that, for low count brain scans in comparison to whole-body PET imaging, much lower β levels (between 100 and 200) are required to achieve the same quantitative results to those obtained with a OSEM method.

The results for all structures, apart from the Substantia Nigra, appeared to be unaffected by the reconstruction method as the changes in the CV were minimal. The Substantia Nigra however appeared to be vulnerable to the reconstruction method under a low count scenario as not only the results appeared more dispersed, but it was also observed an increase of almost 12% for the CV calculation. This finding demonstrates that, when conducting kinetic modelling with an SRTM, the reconstruction algorithm used may have a different impact on different brain structures. This project did not consider partial volume effect correction which is important for small structures such as the Substantia Nigra. Even though Q.Clear improves spatial resolution versus OSEM due to PSF corrections, this is still limited and a consequence of it is the partial volume effect which can affect the PET images quantitatively [23]. Therefore, the results for the Substantia Nigra could be underestimated by a spill-over effect from the white matter located in the midbrain [24].

The penalisation factor in Q.Clear performs as a noise suppression term with higher β values resulting in stronger noise reduction, whilst preserving edges [2,25]. This explains the decrease in the mean BP_{ND} results with the increase in β value, for the SN, St, and GP. The exception to this can be observed in the thalamus as there is a slight increase in the mean BP_{ND} results with the increase in β value, possibly due to the low target density in that region (with BP_{ND} values approximately 10 times lower than high density and large regions, such as the striatum).

The BP_{ND} obtained from the *in vivo* data demonstrates that, in a low count scenario, Q.Clear with β100 has the lowest bias when compared to the standard low count OSEM reconstruction for the SN, GP and Th. For the same metric in the Striatum, Q.Clear with β200 has the lowest bias. Furthermore, when the BP_{ND} for the Cd and Pt are investigated individually it is also noted that Q.Clear with β200 presents the lowest bias for both structures. These results are further substantiated by the multi comparison results which demonstrate that Q.Clear with β100, 200 and 400 are the only reconstructions across all structures that do not present statistically significant ($0.01<p\leq 0.05$), very statistically significant ($0.001<p\leq 0.01$) or extremely statistically significant ($0.0001<p\leq 0.001$) differences when compared to the standard reconstruction.

Lindström et al. (2017) investigated clinical whole-body scans which were acquired in a GE PET-CT system and reconstructed with Q.Clear and TOF-OSEM. They found that in order to obtain a noise equivalence to TOF-OSEM reconstructions with 3iterations, 16subsets and 5mm Gaussian filter, a Q.Clear reconstruction with β600 should be performed for radiotracers such as ^{68}Ga-DOTATOC, ^{18}F-FDG and ^{18}F-Fluoride and a Q.Clear reconstruction with β400 should be performed for ^{11}C-acetate [26].

Scott et al. (2019) aimed at optimising Q.Clear for ^{90}Y quantitative imaging by preparing a National Electrical Manufacturers Association (NEMA) image quality phantom with an ^{90}Y solution and scanning it on a GE Discovery 710 PET-CT scanner. Images were re-binned in the first instance into 15 minute frames and, at a later stage, into 30 and 60 minute frames and reconstructed with Q.Clear with β values of 1, 400, 800, 1000, 1200, 1400, 1600, 1800, 2000, 3000, 4000 and 8000. They calculated activity recovery and found that the optimal value for quantification was β 1000, as the reduction in image noise provided by this reduction does not affect quantification [27].

These reports demonstrate that the optimal β value is dependent on the tracer and the OSEM parameters used for a given application (e.g. brain PET studies versus whole-body PET). Notably, brain PET imaging requires more resolved images and this can be achieved with either an OSEM reconstruction with a high number of iterations and subsets or a Q.Clear reconstruction with low β values. It is encouraging that our results are in line with the report by *Ross (2014)* who reconstructed two ^{18}F-FDG brain image datasets with OSEM 3iterations, 32 subsets and 2.5mm filter and Q.Clear with β150 and found that this β level produced excellent contrast and image quality in both datasets [28]. *Reynés-Llompart et al.* (2018) evaluated phantom and brain and whole-body patient images which had been acquired in a GE Discovery IQ PET-CT system and reconstructed with Q.Clear with β from 50 to 500. They used various acquisition times to mimic different counts – the 15 second acquisition in their study yielded 19 ± 4 million counts, which represents the closest statistics to the ones mimicked in our study. At a 15 second acquisition and using a lesion to background ratio of 2:1, a β value of 150 maximises the contrast to noise ratio (CNR) for a sphere of 10mm, a β value of 200 maximises the CNR for a sphere of 13mm and a β value of 250 maximises the CNR for a sphere of 17mm. Although in kinetic modelling spatial resolution is of more importance than CNR, it is important to note that β values of this range yield good contrast for small structures. Their results also demonstrated that for images of the torso, the optimal β value would be between 300 and 400, whereas for the brain images, it would be between 100 and 200, which is in line with our observation [29]. This suggests that, unlike diagnostic whole-body studies, using ^{18}F-MISO and/or ^{18}F-FAZA in hypoxic lung lesions [13] and ^{18}F-FDG PET-CT in pulmonary nodules [10] , where the optimal β value is 350 and 400 or studies using ^{68}Ga-PSMA and ^{18}F-Fluciclovine in pelvic lesions [30,31] which found that the optimal β value was between 400 and 550 and 300, respectively, for brain studies the optimal β value is lower, particularly when accurate quantification is paramount. In fact, phantom and clinical studies conducted with the aim of improving spatial resolution rather than for diagnostic purposes have reported that Q.Clear with low beta values provides better spatial resolution in small structures. *Rogasch et al (2020)* investigated image metrics such as spatial resolution, contrast recovery and SNR in phantom images reconstructed with Q.Clear and OSEM with PSF modeling. The team found that when using Q.Clear with β 150 and a high signal to background ratio, the spatial resolution obtained is superior to that obtained when reconstructing images with PSF modelling and/or time of flight [9]. Similarly, a publication by *Howard et al (2017)* investigating Q.Clear in small pulmonary nodules reported that Q.Clear with a β value of 150 improved visual conspicuity of nodules of approximately 1cm [14].

Our work follows a similar approach to that of *Teoh et al. (2015), Ter Voert et al. (2018) and Teoh et al. (2018)* [10,30,31]. However, whereas these investigations were performed in whole-body imaging and focusing on the effect of the algorithm on SUV metrics, our work was performed in quantitative dynamic brain imaging and demonstrates the effects on BP_{ND}. To our knowledge, this has not been attempted before. Moreover, our work further sustains the initial observations presented by *Reynés-Llompart et al. (2018)* [29].

A limitation related with the use of Q.Clear that was noted in this study was that for frames with low counts, spurious high counts were seen in the reconstruction and three of the initial frames had to be removed (as was described in the Results section). This demonstrates the importance of the quality control stage in image analysis.

5. Conclusion

In $[^{11}C]$PHNO brain studies that require accurate quantification, Q.Clear with β values between 100 and 200 provide the least bias, lower RC and no statistically significant differences when compared to a standard OSEM reconstruction. Further investigations in this field are required to determine if β values in the range mentioned above provide the same results for other radiopharmaceuticals.

Declarations

Ethics approval and consent to participate

The original study adhered to the principles outlined in the NHS Research Governance Framework for Health and Social Care (2nd edition), the Declaration of Helsinki and Good Clinical Practice (GCP). It was also conducted in compliance with the Protocol, the Data Protection Act and other regulatory requirements and Standard Operating Procedures (SOPs), as appropriate. The data that was used in this project has been acquired after the participant's consent was obtained for the original study (REC reference 12/LO/1955, IRAS Project ID: 103938). Use of this data was covered in the original consent form, which stated that the data acquired could be used in future related research, and therefore ethical approval was waived for this study.

Consent for publication

All patients consented to undergo the original study.

Availability of data and material

The datasets generated and analysed during the current study are not publicly available due to proprietary restrictions but are available from the corresponding author on reasonable request.

Conflicts of interest/Competing interests

The authors declare that they have no competing interests.

Funding

Original study funded by the Medical Research Council (MRC): MC-A656-5QD30.

Code availability

All analysis was done using custom made code at inviCRO, a Konica Minolta Company and is subject to proprietary restrictions on sharing. However, details on fundamentals of this software are described in the manuscript.

Authors' contributions

DR, WH and AAST are responsible for study conception and design. OH, RM and MN are responsible for the submission of the original protocol to relevant entities (ARSAC, REC, HRA) and day to day tasks and management of the study. DR was also responsible for data collection and analysis. All authors contributed equally to data interpretation and manuscript drafting. All authors read and approved the final manuscript.

Acknowledgments

AAST is funded by the British Heart Foundation (FS/19/34/34354).

The authors would like to thank Gaia Rizzo (inviCRO UK) for the excellent support with the MIAKAT software.

List of abbreviations

BPL - Bayesian penalised likelihood

BPND - Binding Potential relative to non-displaceable volume

BSREM - Block Sequential Regularised Expectation Maximisation

Cd - Caudate

CI - Confident Intervals

CT - Computed Tomography

CV - Coefficients of Variation

DARs - D2-like dopaminergic receptors

FBP – Filtered Back Projection

GCP - Good Clinical Practice

GE - General Electric

GP - Globus Pallidus

ICC - Intraclass Correlation Coefficient

MR - Magnetic Resonance

MRAC - MRI-based attenuation correction

NEMA - National Electrical Manufacturers Association

NHS – National Health Service

OSEM - Ordered Subset Expectation Maximisation

PET - Positron Emission Tomography

Pt - Putamen

RC - Repeatability Coefficient

ROI - Region of interest

SN - Substantia Nigra

SNR - Signal to Noise Ratio

SOPs - Standard Operating Procedures

SRTM - Simplified Reference Tissue Model

St - Striatum

TACs - Time Activity Curves

TE - Echo Time

Th - Thalamus

ToF - Time of Flight

TR - Repetition Time

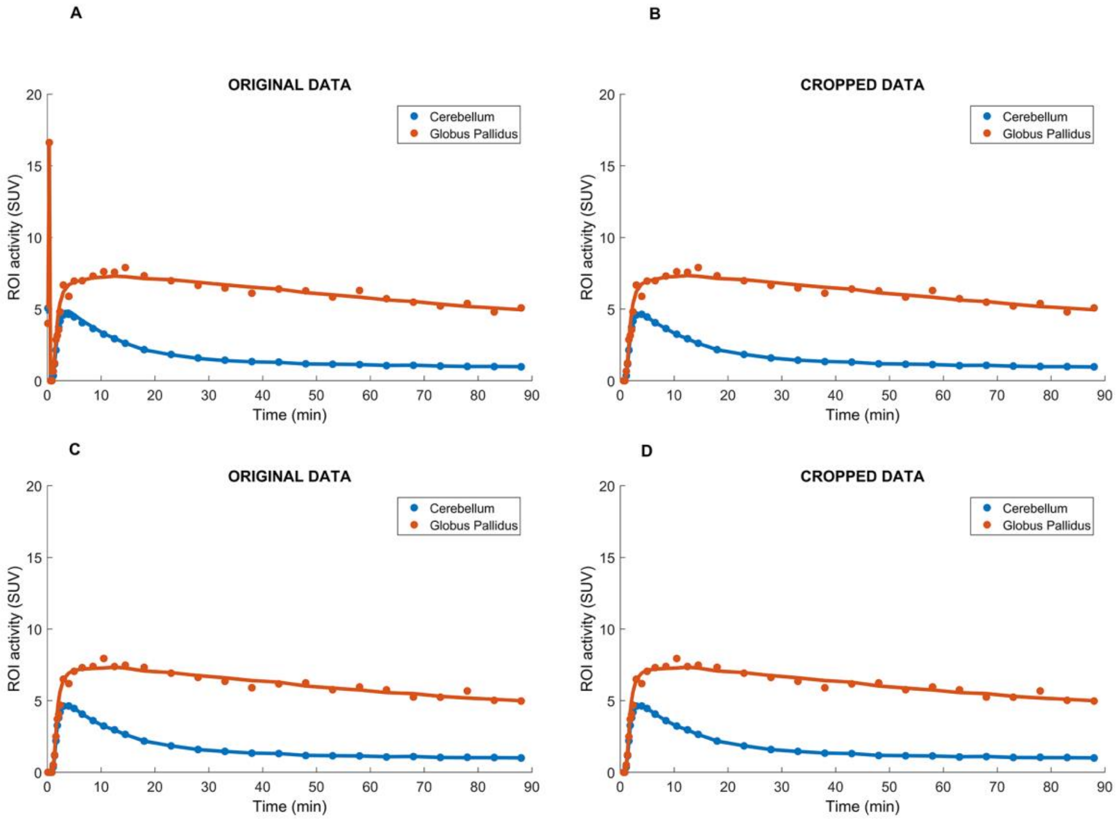

Fig. 1 Model fitting obtained for the Cerebellum and Globus Pallidus, one PET-MR brain dataset (same subject) reconstructed with TOF Q.Clear β100 (top row) and OSEM (bottom row). Note the interference of the background counts on the model fitting on the graphic entitled "Original Data" (A). The three initial frames that contained background counts were removed on the graphic entitled "Cropped data" (B). Note the lack of interference from the background counts, when OSEM is used, on the model fitting on graphic (C) and the similar model fitting obtained when the initial frames are removed for the OSEM reconstructed, on graphic (D).

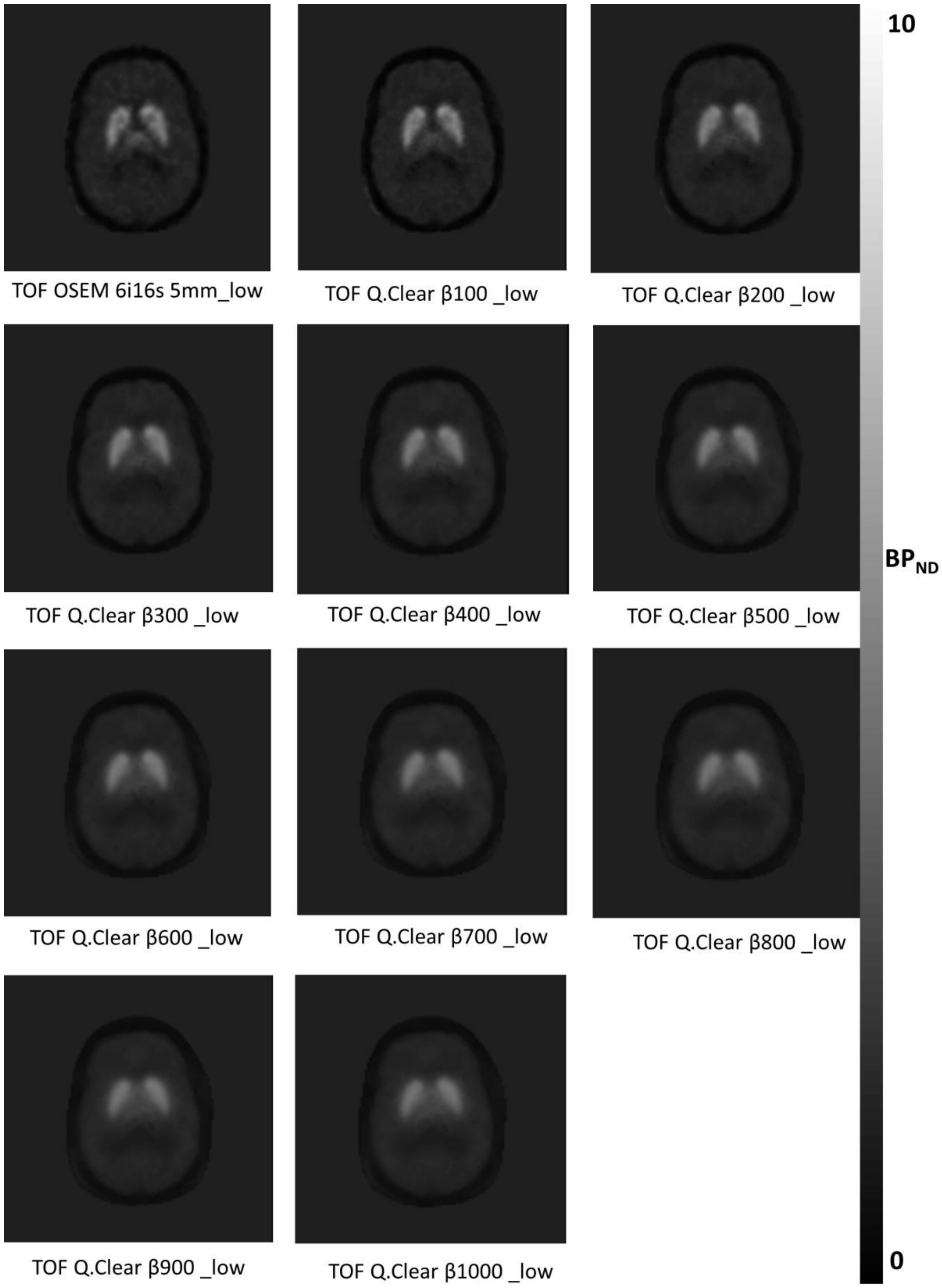

Fig. 2 Representative BP_{ND} parametric brain images after [^{11}C]PHNO administration, per reconstruction method under low counts. Note the visual differences in image quality for the Q.Clear reconstructions as β increases.

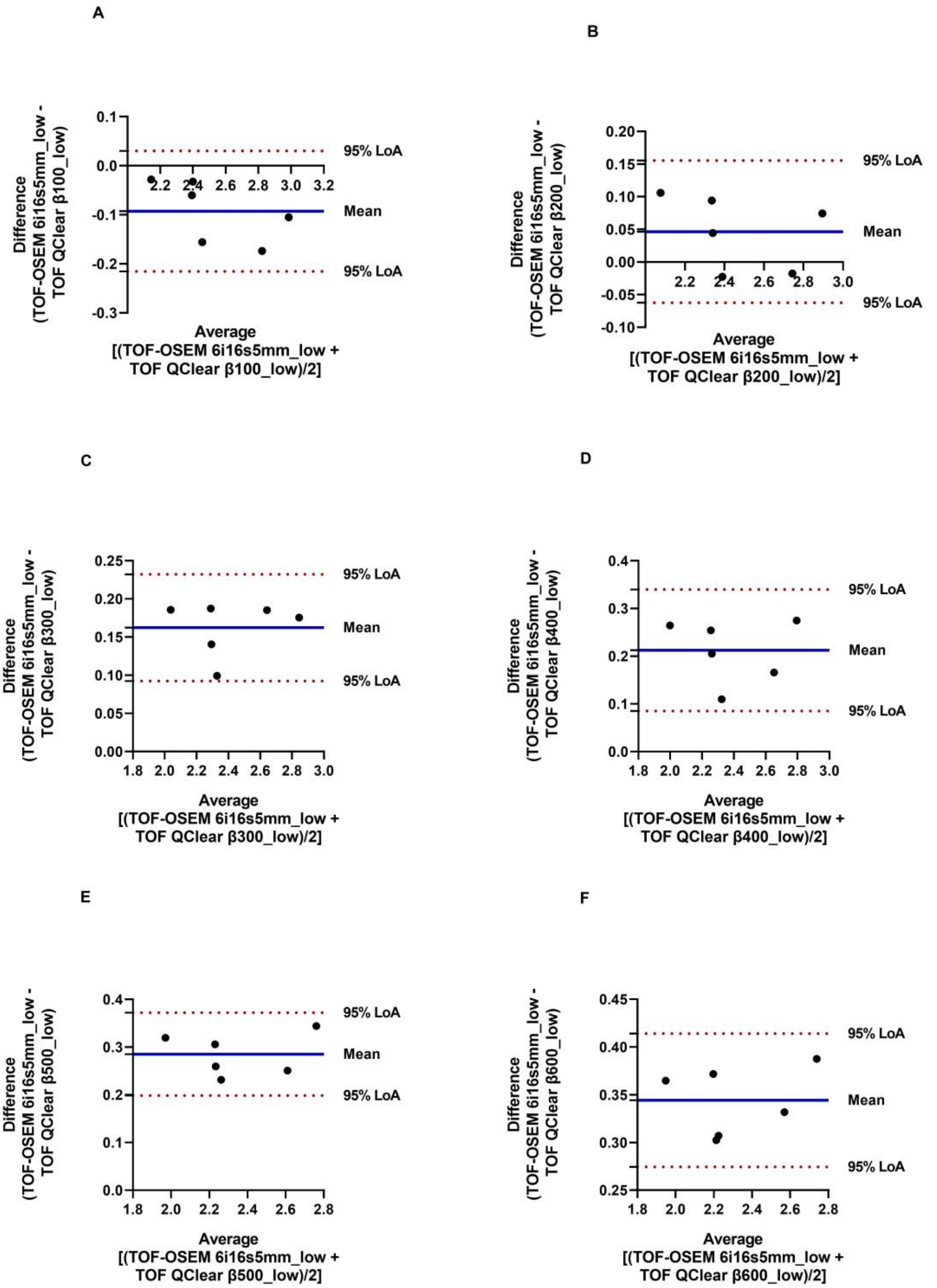

LoA = Limits of Agreement

Fig. 3 Bland-Altman plots of the BP_{ND} obtained for the Striatum: **(A)** – TOF OSEM 6i16s5mm_low vs TOF Q.Clear β100_low; **(B)** – TOF OSEM 6i16s5mm _low vs TOF Q.Clear β200_low; **(C)** – TOF OSEM 6i16s5mm_low vs TOF Q.Clear β300_low; **(D)** – TOF OSEM 6i16s5mm _low vs TOF Q.Clear β400_low; **(E)** – TOF OSEM 6i16s5mm_low vs TOF Q.Clear β500_low; **(F)** – TOF OSEM 6i16s5mm_low vs TOF Q.Clear β600_low.

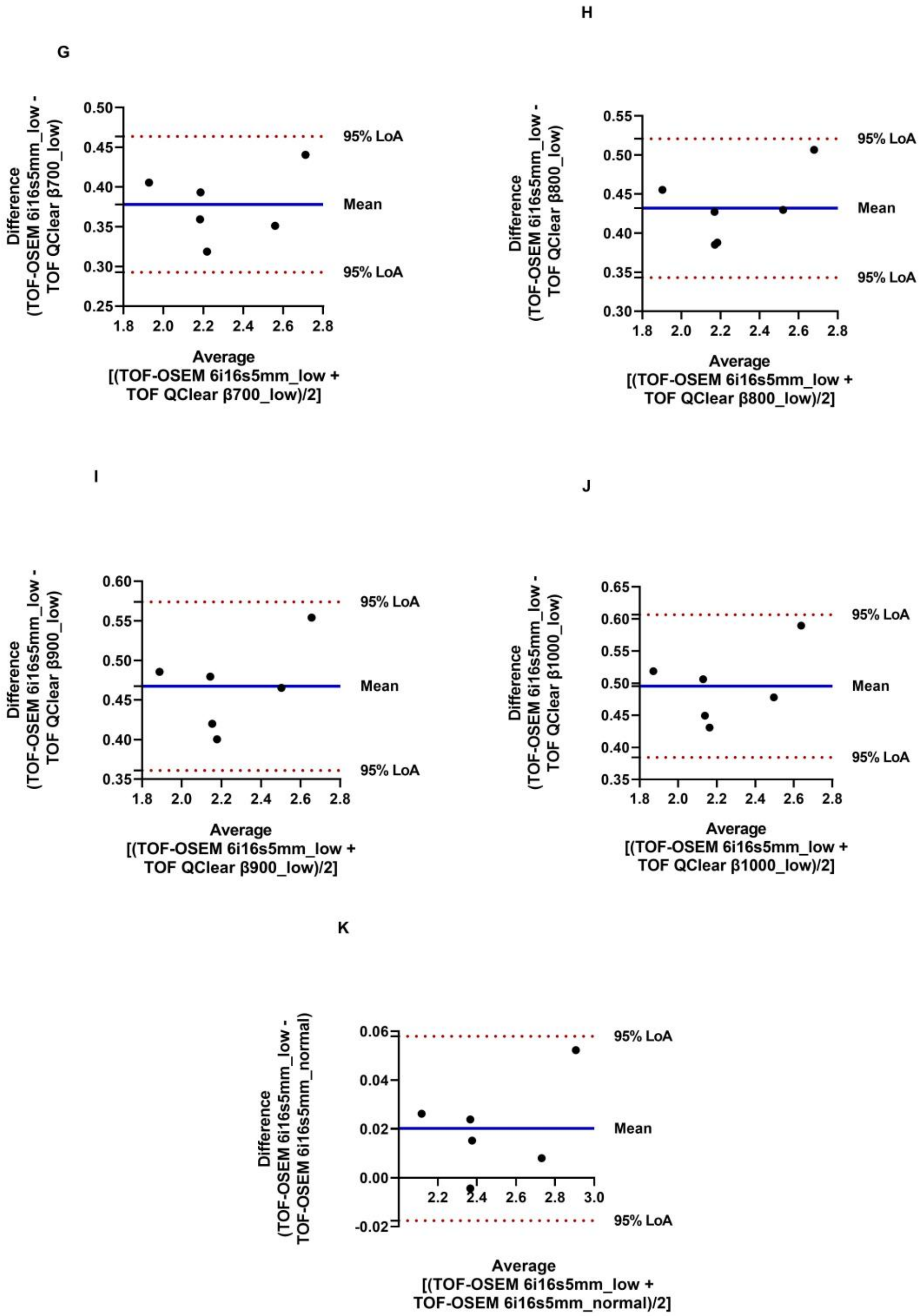

LoA = Limits of Agreement

Fig. 4 Bland-Altman plots of the BP_{ND} obtained for the Striatum: **(G)** – TOF OSEM 6i16s5mm _low vs TOF Q.Clear β700_low; **(H)** – TOF OSEM 6i16s5mm _low vs TOF Q.Clear β800_low; **(I)** – TOF OSEM 6i16s5mm_low vs TOF Q.Clear β900_low; **(J)** – TOF OSEM 6i16s5mm _low vs TOF Q.Clear β1000_low; **(K)** – TOF OSEM 6i16s5mm _low vs TOF OSEM 6i16s5mm_normal

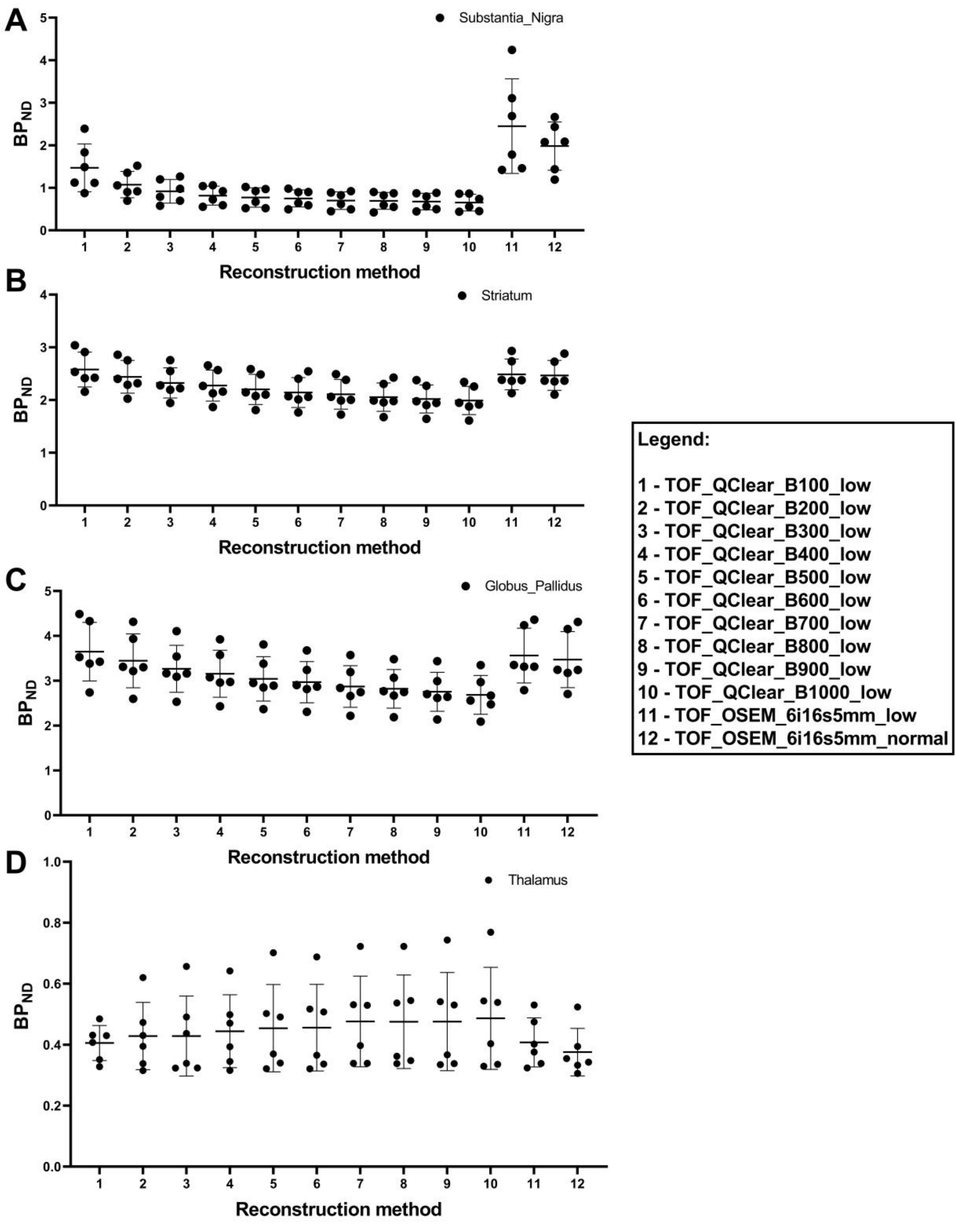

Fig. 5 Graphic layout of the BP_{ND} obtained for the Substantia Nigra **(A)**, Striatum **(B)**, Globus Pallidus **(C)** and Thalamus **(D)**, per reconstruction method. For the Substantia Nigra **(A)**, Striatum **(B)** and Globus Pallidus **(C)** as the β value for the Q.Clear reconstructions increases, the mean BP_{ND} decreases. However, for the Thalamus **(D)**, as the β value for the Q.Clear reconstructions increases, the mean BP_{ND} **increases**.

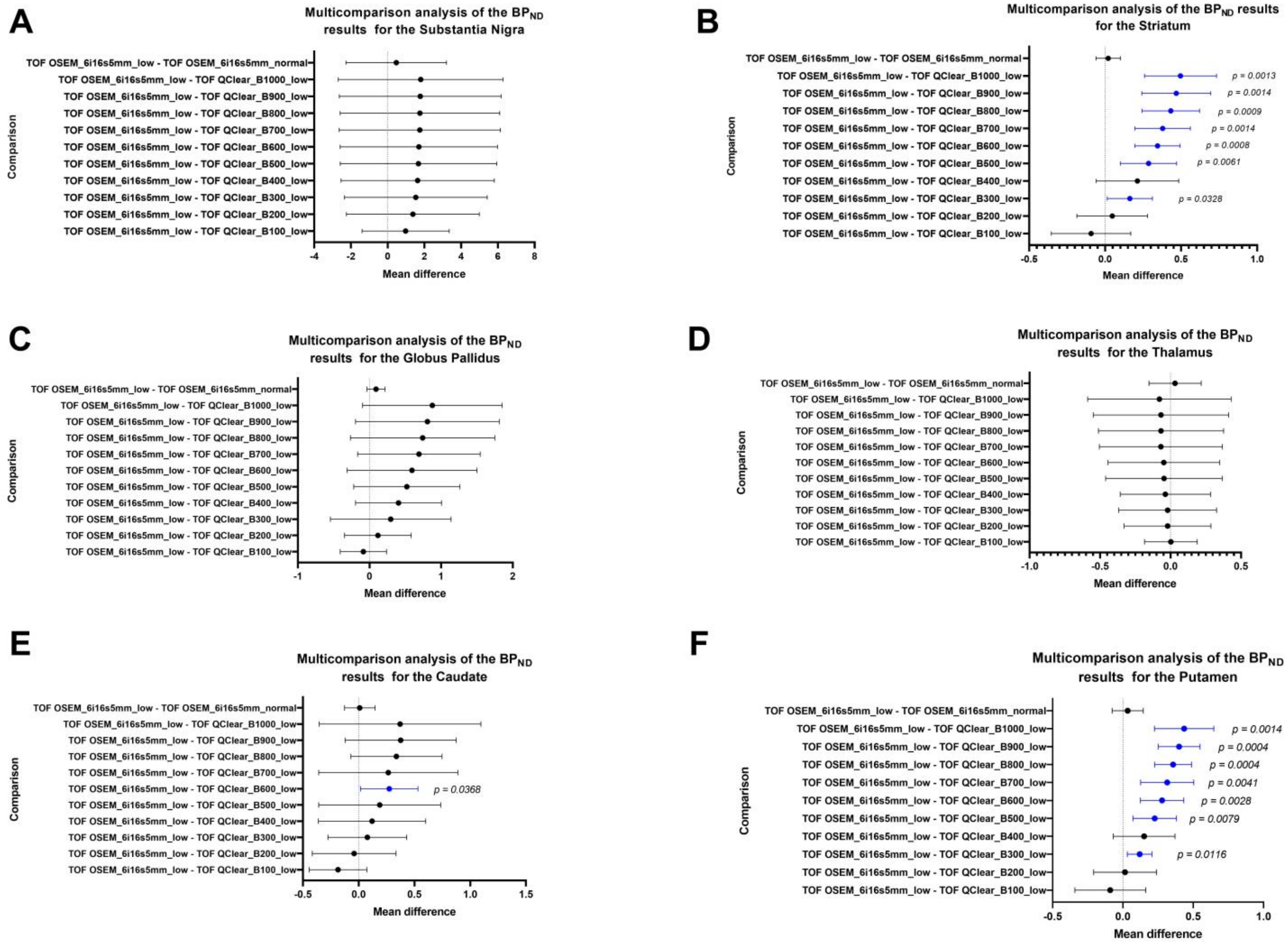

Fig. 6 Multicomparison analysis of the BP_{ND} results obtained for all structures when images reconstructed the standard OSEM 6iterations 16subsets and 5mm filter and with the Q.Clear reconstructions with different β values. Note the statistically significant results included on the graphs.

References

1. Reilhac A, Tomeï S, Buvat I, Michel C, Keheren F, Costes N. Simulation-based evaluation of OSEM iterative reconstruction methods in dynamic brain PET studies. NeuroImage. 2008;39:359–68.

2. te Riet J, Rijnsdorp S, Roef MJ, Arends AJ. Evaluation of a Bayesian penalized likelihood reconstruction algorithm for low-count clinical 18F-FDG PET/CT. EJNMMI Physics. 2019;6:32.

3. Boellaard R, van Lingen A, Lammertsma AA. Experimental and Clinical Evaluation of Iterative Reconstruction (OSEM) in Dynamic PET: Quantitative Characteristics and Effects on Kinetic Modeling. Journal of Nuclear Medicine [Internet]. 2001;42:808. Available from: http://jnm.snmjournals.org/content/42/5/808.abstract

4. Riddell C, Carson RE, Carrasquillo JA, Libutti SK, Danforth DN, Whatley M, et al. Noise Reduction in Oncology FDG PET Images by Iterative Reconstruction: A Quantitative Assessment. Journal of Nuclear Medicine [Internet]. 2001;42:1316 LP – 1323. Available from: http://jnm.snmjournals.org/content/42/9/1316.abstract

5. Richter D, Basse-Lüsebrink TC, Kampf T, Fischer A, Israel I, Schneider M, et al. Compressed sensing for reduction of noise and artefacts in direct PET image reconstruction. Zeitschrift für Medizinische Physik [Internet]. 2014;24:16–26. Available from: https://www.sciencedirect.com/science/article/pii/S0939388913000640

6. Otani T, Hosono M, Kanagaki M. Clinical evaluation and optimization of Q.Clear; a new PET reconstruction algorithm. Journal of Nuclear Medicine. 2017;58:575 LP – 575.

7. Ribeiro D, Hallett W, Tavares AAS. Performance evaluation of the Q.Clear reconstruction framework versus conventional reconstruction algorithms for quantitative brain PET-MR studies. EJNMMI Physics [Internet]. 2021;8:41. Available from: https://doi.org/10.1186/s40658-021-00386-3

8. Ziai P, Hayeri MR, Salei A, Salavati A, Houshmand S, Alavi A, et al. Role of Optimal Quantification of FDG PET Imaging in the Clinical Practice of Radiology. RadioGraphics. Radiological Society of North America; 2016;36:481–96.

9. Rogasch JM, Suleiman S, Hofheinz F, Bluemel S, Lukas M, Amthauer H, et al. Reconstructed spatial resolution and contrast recovery with Bayesian penalized likelihood reconstruction (Q.Clear) for FDG-PET compared to time-of-flight (TOF) with point spread function (PSF). EJNMMI Physics [Internet]. 2020;7:2. Available from: https://doi.org/10.1186/s40658-020-0270-y

10. Teoh EJ, McGowan DR, Macpherson RE, Bradley KM, Gleeson F v. Phantom and clinical evaluation of the Bayesian penalized likelihood reconstruction algorithm Q.Clear on an LYSO PET/CT system. Journal of nuclear medicine : official publication, Society of Nuclear Medicine [Internet]. 2015;56:1447–52. Available from: https://www.ncbi.nlm.nih.gov/pmc/articles/PMC4558942/

11. Wyrzykowski M, Siminiak N, Kaźmierczak M, Ruchała M, Czepczyński R. Impact of the Q.Clear reconstruction algorithm on the interpretation of PET/CT images in patients with lymphoma. EJNMMI research. Springer Berlin Heidelberg; 2020;10:99.

12. Witkowska-Patena E, Budzyńska A, Giżewska A, Dziuk M, Walęcka-Mazur A. Ordered subset expectation maximisation vs Bayesian penalised likelihood reconstruction algorithm in 18F-PSMA-1007 PET/CT. Annals of Nuclear Medicine. 2020;34:192–9.

13. Texte E, Gouel P, Thureau S, Lequesne J, Barres B, Edet-Sanson A, et al. Impact of the Bayesian penalized likelihood algorithm (Q.Clear®) in comparison with the OSEM reconstruction on low contrast PET hypoxic images. EJNMMI Physics [Internet]. 2020;7:28. Available from: https://doi.org/10.1186/s40658-020-00300-3

14. Howard BA, Morgan R, Thorpe MP, Turkington TG, Oldan J, James OG, et al. Comparison of Bayesian penalized likelihood reconstruction versus OS-EM for characterization of small pulmonary nodules in oncologic PET/CT. Annals of Nuclear Medicine [Internet]. 2017;31:623–8. Available from: https://doi.org/10.1007/s12149-017-1192-1

15. Rangel-Barajas C, Coronel I, Florán B. Dopamine Receptors and Neurodegeneration. Aging and disease. JKL International LLC; 2015;6:349–68.

16. Dahoun T, Nour MM, McCutcheon RA, Adams RA, Bloomfield MAP, Howes OD. The relationship between childhood trauma, dopamine release and dexamphetamine-induced positive psychotic symptoms: a [(11)C]-(+)-PHNO PET study. Translational psychiatry. Nature Publishing Group UK; 2019;9:287.

17. Howes O, McCutcheon R, Stone J. Glutamate and dopamine in schizophrenia: an update for the 21st century. Journal of psychopharmacology (Oxford, England). 2015/01/13. 2015;29:97–115.

18. Colom M, Vidal B, Zimmer L. Is There a Role for GPCR Agonist Radiotracers in PET Neuroimaging? Frontiers in molecular neuroscience. Frontiers Media S.A.; 2019;12:255.

19. Nour MM, Dahoun T, Schwartenbeck P, Adams RA, FitzGerald THB, Coello C, et al. Dopaminergic basis for signaling belief updates, but not surprise, and the link to paranoia. Proceedings of the National Academy of Sciences. 2018;115:E10167 LP-E10176.

20. Salinas CA, Searle GE, Gunn RN. The simplified reference tissue model: model assumption violations and their impact on binding potential. Journal of cerebral blood flow and metabolism : official journal of the International Society of Cerebral Blood Flow and Metabolism. 2015;35:304–11.

21. Varrone A, Asenbaum S, Vander Borght T, Booij J, Nobili F, Någren K, et al. EANM procedure guidelines for PET brain imaging using [18F]FDG, version 2. European journal of nuclear medicine and molecular imaging. Germany; 2009;36:2103–10.

22. Maguire RP, Leenders KL. PET Pharmacokinetic Course Manual [Internet]. 2003 [cited 2020 Jun 11]. p. 158. Available from: www.bic.mni.mcgill.ca/~rgunn/PK_Course_2003/PKM_Manual_Web.pdf

23. Rogasch JM, Suleiman S, Hofheinz F, Bluemel S, Lukas M, Amthauer H, et al. Reconstructed spatial resolution and contrast recovery with Bayesian penalized likelihood reconstruction (Q.Clear) for FDG-PET compared to time-of-flight (TOF) with point spread function (PSF). EJNMMI Physics. 2020;7:2.

24. Graff-Guerrero A, Willeit M, Ginovart N, Mamo D, Mizrahi R, Rusjan P, et al. Brain region binding of the D2/3 agonist [11C]-(+)-PHNO and the D2/3 antagonist [11C]raclopride in healthy humans. Human Brain Mapping. John Wiley & Sons, Ltd; 2008;29:400–10.

25. Kim HS, Cho S-G, Kim JH, Kwon SY, Lee B-I, Bom H-S. Effect of Post-Reconstruction Gaussian Filtering on Image Quality and Myocardial Blood Flow Measurement with N-13 Ammonia PET. Asia Oceania journal of nuclear medicine & biology. Asia Oceania Journal of Nuclear Medicine & Biology; 2014;2:104–10.

26. LindstrÃ¶m E, LindsjÃ¶ L, Ilan E, Sundin A, Sorensen J, Danfors T, et al. Optimisation of penalized likelihood estimation reconstruction (Q.Clear) on a digital time-of-flight PET-CT scanner for four different PET tracers. Journal of Nuclear Medicine. 2017;58:1355 LP – 1355.

27. Scott NP, McGowan DR. Optimising quantitative 90Y PET imaging: an investigation into the effects of scan length and Bayesian penalised likelihood reconstruction. EJNMMI Research. 2019;9:40.

28. Ross S. Q.Clear - GE Healthcare [Internet]. 2014 [cited 2019 Apr 7]. p. 9. Available from: https://www.gehealthcare.com.sg/-/jssmedia/739d885baa59485aaef5ac0e0eeb44a4.pdf

29. Reynés-Llompart G, Gámez-Cenzano C, Vercher-Conejero JL, Sabaté-Llobera A, Calvo-Malvar N, Martí-Climent JM. Phantom, clinical, and texture indices evaluation and optimization of a penalized-likelihood image reconstruction method (Q.Clear) on a BGO PET/CT scanner. Medical Physics. John Wiley & Sons, Ltd; 2018;45:3214–22.

30. ter Voert EEGW, Muehlematter UJ, Delso G, Pizzuto DA, Müller J, Nagel HW, et al. Quantitative performance and optimal regularization parameter in block sequential regularized expectation maximization reconstructions in clinical (68)Ga-PSMA PET/MR. EJNMMI research [Internet]. Springer Berlin Heidelberg; 2018;8:70. Available from: https://pubmed.ncbi.nlm.nih.gov/30054750

31. Teoh EJ, McGowan DR, Schuster DM, Tsakok MT, Gleeson F v, Bradley KM. Bayesian penalised likelihood reconstruction (Q.Clear) of (18)F-fluciclovine PET for imaging of recurrent prostate cancer: semi-quantitative and clinical evaluation. The British journal of radiology [Internet]. 2018/01/22. The British Institute of Radiology.; 2018;91:20170727. Available from: https://pubmed.ncbi.nlm.nih.gov/29303359

Supplementary File 1

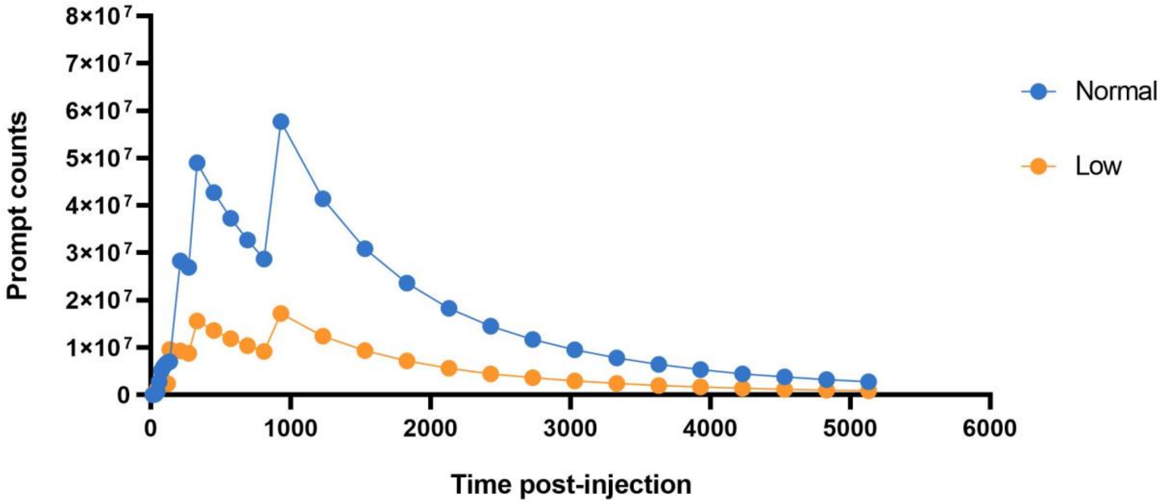

Fig. 1 Graphic of the prompt events over time (time post-injection). Note the higher prompt counts for the plot denominated "normal", which refers to the datasets with normal counts. The plot denominated "low" refers to the datasets in which low counts were simulated. Both plots belong to the same participant.

Supplementary File 2

Table 1

Table 1 *Bias, Standard deviation of Bias, Repeatability Coefficients (RC), Lower Limits of Agreement (LoA), Higher LoA,, standard deviation of Bias and LoA obtained, per brain structure, when Q.Clear reconstructions with pre-frame delay and OSEM reconstruction with normal frame length were compared to standard OSEM reconstruction with pre-frame delay.*

		Bias	SD Bias	RC	Lower LoA	Higher LoA
SN						
	TOF_OSEM6i16s5mm_low vs TOF_Q.Clear 100_low	0.979	0.568	2.172	-0.135	2.093
	TOF_OSEM6i16s5mm_low vs TOF_Q.Clear 200_low	1.376	0.867	3.110	-0.323	3.074
	TOF_OSEM6i16s5mm_low vs TOF_Q.Clear 300_low	1.533	0.931	3.435	-0.293	3.358
	TOF_OSEM6i16s5mm_low vs TOF_Q.Clear 400_low	1.634	1.000	3.668	-0.326	3.593
	TOF_OSEM6i16s5mm_low vs TOF_Q.Clear 500_low	1.679	1.021	3.763	-0.322	3.679
	TOF_OSEM6i16s5mm_low vs TOF_Q.Clear 600_low	1.699	1.027	3.804	-0.313	3.712
	TOF_OSEM6i16s5mm_low vs TOF_Q.Clear 700_low	1.751	1.052	3.914	-0.310	3.812
	TOF_OSEM6i16s5mm_low vs TOF_Q.Clear 800_low	1.756	1.040	3.914	-0.283	3.796
	TOF_OSEM6i16s5mm_low vs TOF_Q.Clear 900_low	1.773	1.055	3.955	-0.293	3.840
	TOF_OSEM6i16s5mm_low vs TOF_Q.Clear 1000_low	1.798	1.075	4.015	-0.308	3.904
	TOF_OSEM6i16s5mm_low vs TOF_OSEM6i16s5mm_normal	0.469	0.656	1.490	-0.817	1.754
St						
	TOF_OSEM6i16s5mm_low vs TOF_Q.Clear 100_low	-0.093	0.063	0.213	-0.215	0.030
	TOF_OSEM6i16s5mm_low vs TOF_Q.Clear 200_low	0.046	0.056	0.135	-0.062	0.155
	TOF_OSEM6i16s5mm_low vs TOF_Q.Clear 300_low	0.162	0.036	0.324	0.092	0.232
	TOF_OSEM6i16s5mm_low vs TOF_Q.Clear 400_low	0.213	0.065	0.432	0.085	0.340
	TOF_OSEM6i16s5mm_low vs TOF_Q.Clear 500_low	0.285	0.044	0.565	0.198	0.372
	TOF_OSEM6i16s5mm_low vs TOF_Q.Clear 600_low	0.344	0.036	0.678	0.274	0.414
	TOF_OSEM6i16s5mm_low vs TOF_Q.Clear 700_low	0.378	0.044	0.745	0.293	0.464
	TOF_OSEM6i16s5mm_low vs TOF_Q.Clear 800_low	0.432	0.045	0.851	0.343	0.521
	TOF_OSEM6i16s5mm_low vs TOF_Q.Clear 900_low	0.468	0.054	0.921	0.361	0.574
	TOF_OSEM6i16s5mm_low vs TOF_Q.Clear 1000_low	0.496	0.057	0.976	0.384	0.607
	TOF_OSEM6i16s5mm_low vs TOF_OSEM6i16s5mm_normal	0.020	0.019	0.053	-0.018	0.058
GP						
	TOF_OSEM6i16s5mm_low vs TOF_Q.Clear 100_low	-0.087	0.077	0.220	-0.239	0.065
	TOF_OSEM6i16s5mm_low vs TOF_Q.Clear 200_low	0.116	0.112	0.303	-0.103	0.335
	TOF_OSEM6i16s5mm_low vs TOF_Q.Clear 300_low	0.295	0.202	0.682	-0.100	0.691
	TOF_OSEM6i16s5mm_low vs TOF_Q.Clear 400_low	0.405	0.144	0.834	0.123	0.687
	TOF_OSEM6i16s5mm_low vs TOF_Q.Clear 500_low	0.521	0.178	1.069	0.172	0.869
	TOF_OSEM6i16s5mm_low vs TOF_Q.Clear 600_low	0.593	0.217	1.226	0.167	1.019

	TOF_OSEM6i16s5mm_low vs TOF_Q.Clear 700_low	0.690	0.205	1.401	0.288	1.091
	TOF_OSEM6i16s5mm_low vs TOF_Q.Clear 800_low	0.741	0.242	1.515	0.268	1.215
	TOF_OSEM6i16s5mm_low vs TOF_Q.Clear 900_low	0.808	0.241	1.641	0.336	1.279
	TOF_OSEM6i16s5mm_low vs TOF_Q.Clear 1000_low	0.876	0.233	1.768	0.419	1.334
	TOF_OSEM6i16s5mm_low vs TOF_OSEM6i16s5mm_normal	0.090	0.030	0.185	0.031	0.149
Th						
	TOF_OSEM6i16s5mm_low vs TOF_Q.Clear 100_low	0.002	0.045	0.080	-0.086	0.090
	TOF_OSEM6i16s5mm_low vs TOF_Q.Clear 200_low	-0.021	0.074	0.138	-0.166	0.124
	TOF_OSEM6i16s5mm_low vs TOF_Q.Clear 300_low	-0.021	0.083	0.155	-0.184	0.143
	TOF_OSEM6i16s5mm_low vs TOF_Q.Clear 400_low	-0.037	0.077	0.155	-0.187	0.114
	TOF_OSEM6i16s5mm_low vs TOF_Q.Clear 500_low	-0.047	0.099	0.200	-0.241	0.148
	TOF_OSEM6i16s5mm_low vs TOF_Q.Clear 600_low	-0.048	0.095	0.194	-0.234	0.138
	TOF_OSEM6i16s5mm_low vs TOF_Q.Clear 700_low	-0.069	0.105	0.231	-0.274	0.136
	TOF_OSEM6i16s5mm_low vs TOF_Q.Clear 800_low	-0.068	0.107	0.232	-0.277	0.141
	TOF_OSEM6i16s5mm_low vs TOF_Q.Clear 900_low	-0.068	0.115	0.246	-0.294	0.158
	TOF_OSEM6i16s5mm_low vs TOF_Q.Clear 1000_low	-0.079	0.122	0.268	-0.318	0.160
	TOF_OSEM6i16s5mm_low vs TOF_OSEM6i16s5mm_normal	0.032	0.044	0.101	-0.055	0.119
Cd						
	TOF_OSEM6i16s5mm_low vs TOF_Q.Clear 100_low	-0.185	0.062	0.380	-0.307	-0.064
	TOF_OSEM6i16s5mm_low vs TOF_Q.Clear 200_low	-0.041	0.090	0.180	-0.217	0.136
	TOF_OSEM6i16s5mm_low vs TOF_Q.Clear 300_low	0.078	0.085	0.215	-0.088	0.244
	TOF_OSEM6i16s5mm_low vs TOF_Q.Clear 400_low	0.120	0.115	0.313	-0.106	0.346
	TOF_OSEM6i16s5mm_low vs TOF_Q.Clear 500_low	0.189	0.131	0.438	-0.068	0.445
	TOF_OSEM6i16s5mm_low vs TOF_Q.Clear 600_low	0.275	0.062	0.549	0.154	0.396
	TOF_OSEM6i16s5mm_low vs TOF_Q.Clear 700_low	0.266	0.150	0.585	-0.028	0.559
	TOF_OSEM6i16s5mm_low vs TOF_Q.Clear 800_low	0.339	0.098	0.686	0.147	0.531
	TOF_OSEM6i16s5mm_low vs TOF_Q.Clear 900_low	0.377	0.119	0.769	0.143	0.611
	TOF_OSEM6i16s5mm_low vs TOF_Q.Clear 1000_low	0.372	0.174	0.792	0.031	0.712
	TOF_OSEM6i16s5mm_low vs TOF_OSEM6i16s5mm_normal	0.010	0.033	0.062	-0.054	0.074
Pt						
	TOF_OSEM6i16s5mm_low vs TOF_Q.Clear 100_low	-0.090	0.060	0.208	-0.209	0.028
	TOF_OSEM6i16s5mm_low vs TOF_Q.Clear 200_low	0.015	0.054	0.100	-0.090	0.120
	TOF_OSEM6i16s5mm_low vs TOF_Q.Clear 300_low	0.119	0.021	0.236	0.077	0.160
	TOF_OSEM6i16s5mm_low vs TOF_Q.Clear 400_low	0.151	0.053	0.310	0.048	0.254
	TOF_OSEM6i16s5mm_low vs TOF_Q.Clear 500_low	0.226	0.037	0.447	0.153	0.298
	TOF_OSEM6i16s5mm_low vs TOF_Q.Clear 600_low	0.278	0.037	0.549	0.206	0.351
	TOF_OSEM6i16s5mm_low vs TOF_Q.Clear 700_low	0.315	0.045	0.622	0.226	0.404
	TOF_OSEM6i16s5mm_low vs TOF_Q.Clear 800_low	0.356	0.031	0.701	0.295	0.418
	TOF_OSEM6i16s5mm_low vs TOF_Q.Clear 900_low	0.399	0.036	0.784	0.329	0.469
	TOF_OSEM6i16s5mm_low vs TOF_Q.Clear 1000_low	0.435	0.051	0.858	0.336	0.534
	TOF_OSEM6i16s5mm_low vs TOF_OSEM6i16s5mm_normal	0.034	0.027	0.081	-0.018	0.086

Supplementary File 3

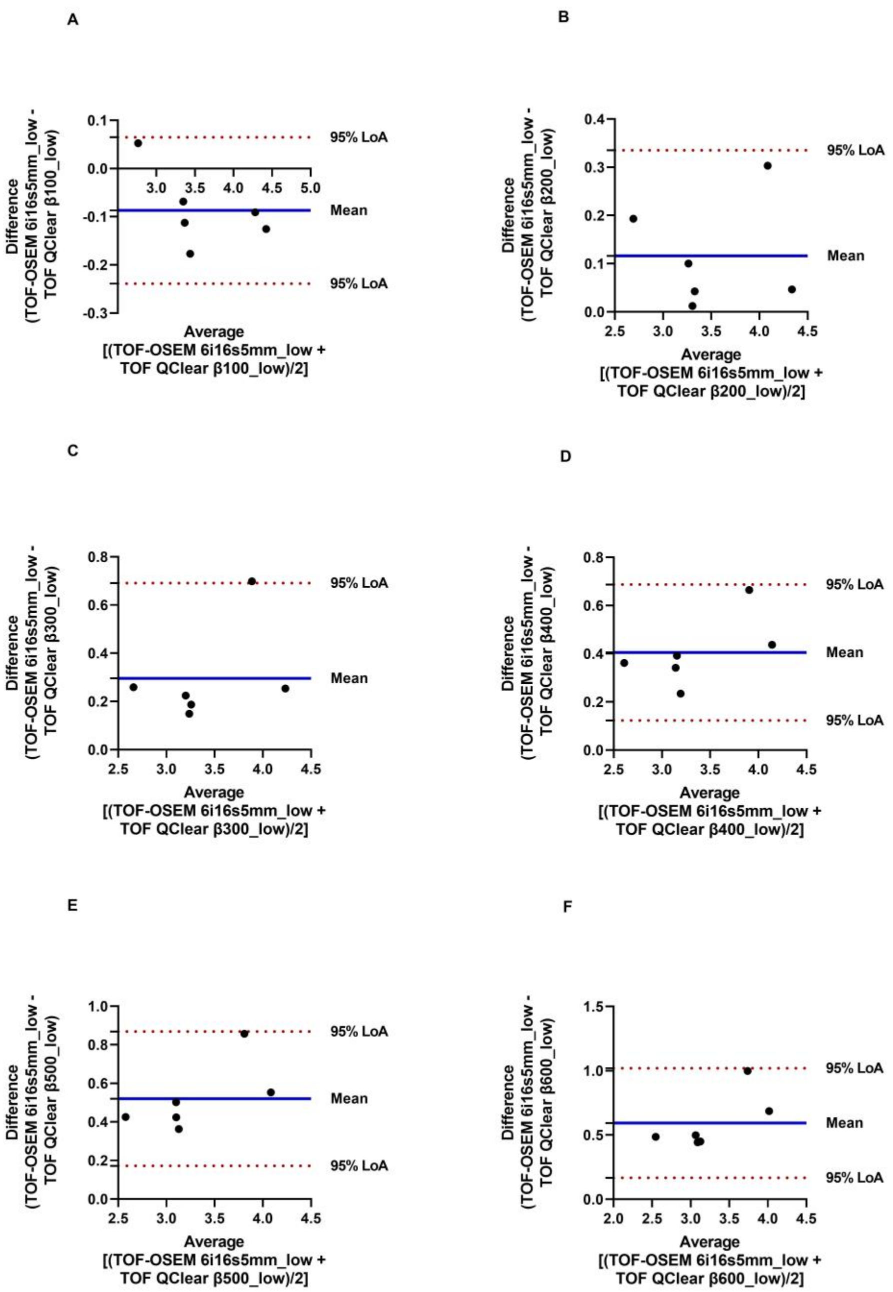

LoA = Limits of Agreement

Fig. 1 Bland-Altman plots of the BP_{ND} obtained for the Globus Pallidus: **(A)** – TOF_OSEM 6i16s5mm_low vs TOF_Q.Clear β100_low; **(B)** - TOF_OSEM 6i16s5mm _low vs TOF_Q.Clear β200_low; **(C)** - TOF_OSEM 6i16s5mm_low vs TOF_Q.Clear β300_low; **(D)** - TOF_OSEM 6i16s5mm _low vs TOF_Q.Clear β400_low; **(E)** - TOF_OSEM 6i16s5mm_low vs TOF_Q.Clear β500_low; **(F)** - TOF_OSEM 6i16s5mm_low vs TOF_Q.Clear β600_low.

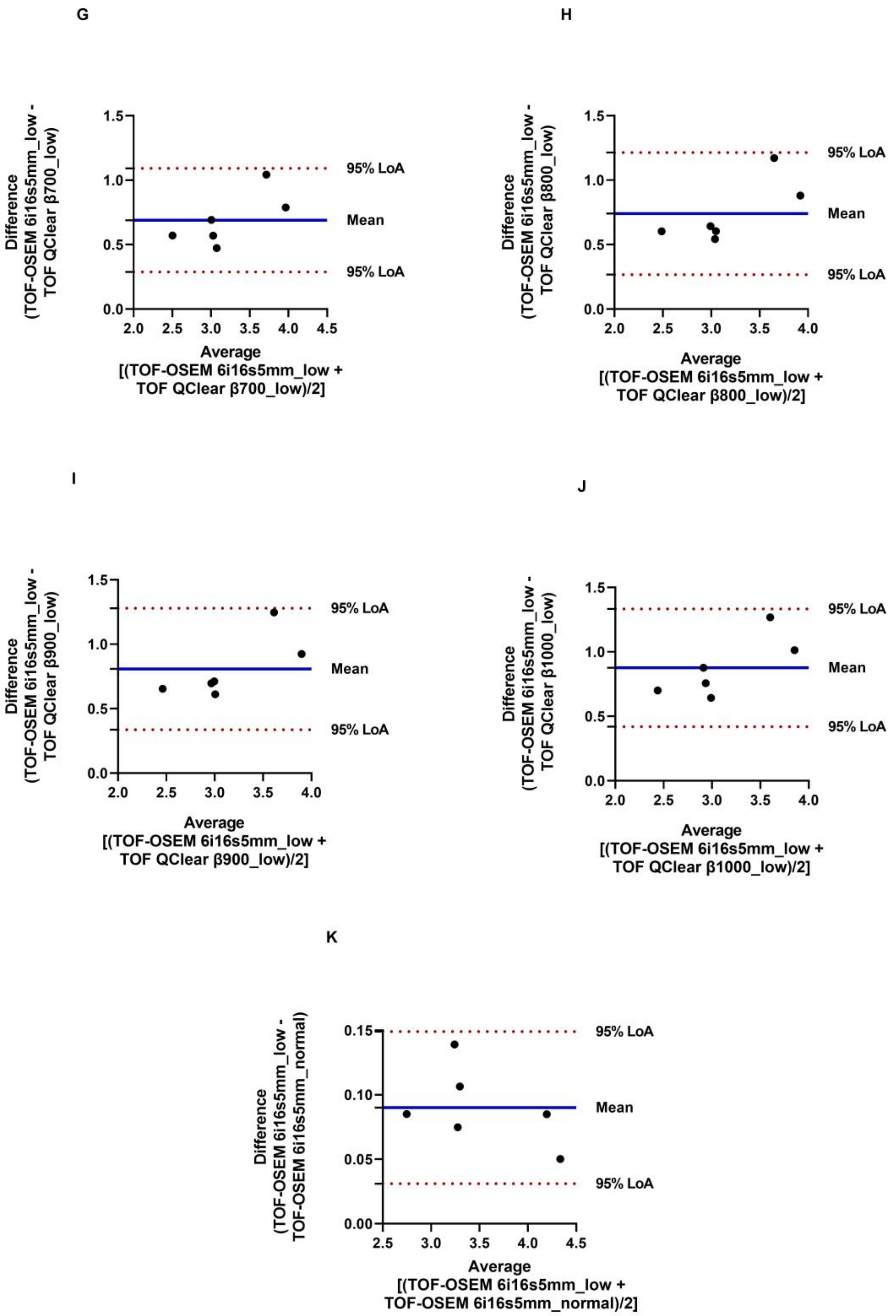

LoA = Limits of Agreement

Fig. 2 Bland-Altman plots of the BP_{ND} obtained for the Globus Pallidus: **(G)** - TOF_OSEM 6i16s5mm _low vs TOF_Q.Clear β700_low; **(H)** - TOF_OSEM 6i16s5mm _low vs TOF_Q.Clear β800_low; **(I)** - TOF_OSEM 6i16s5mm_low vs TOF_Q.Clear β900_low; **(J)** - TOF_OSEM 6i16s5mm _low vs TOF_Q.Clear β1000_low; **(K)** - TOF_OSEM 6i16s5mm _low vs TOF_OSEM 6i16s5mm_normal.

Supplementary File 4

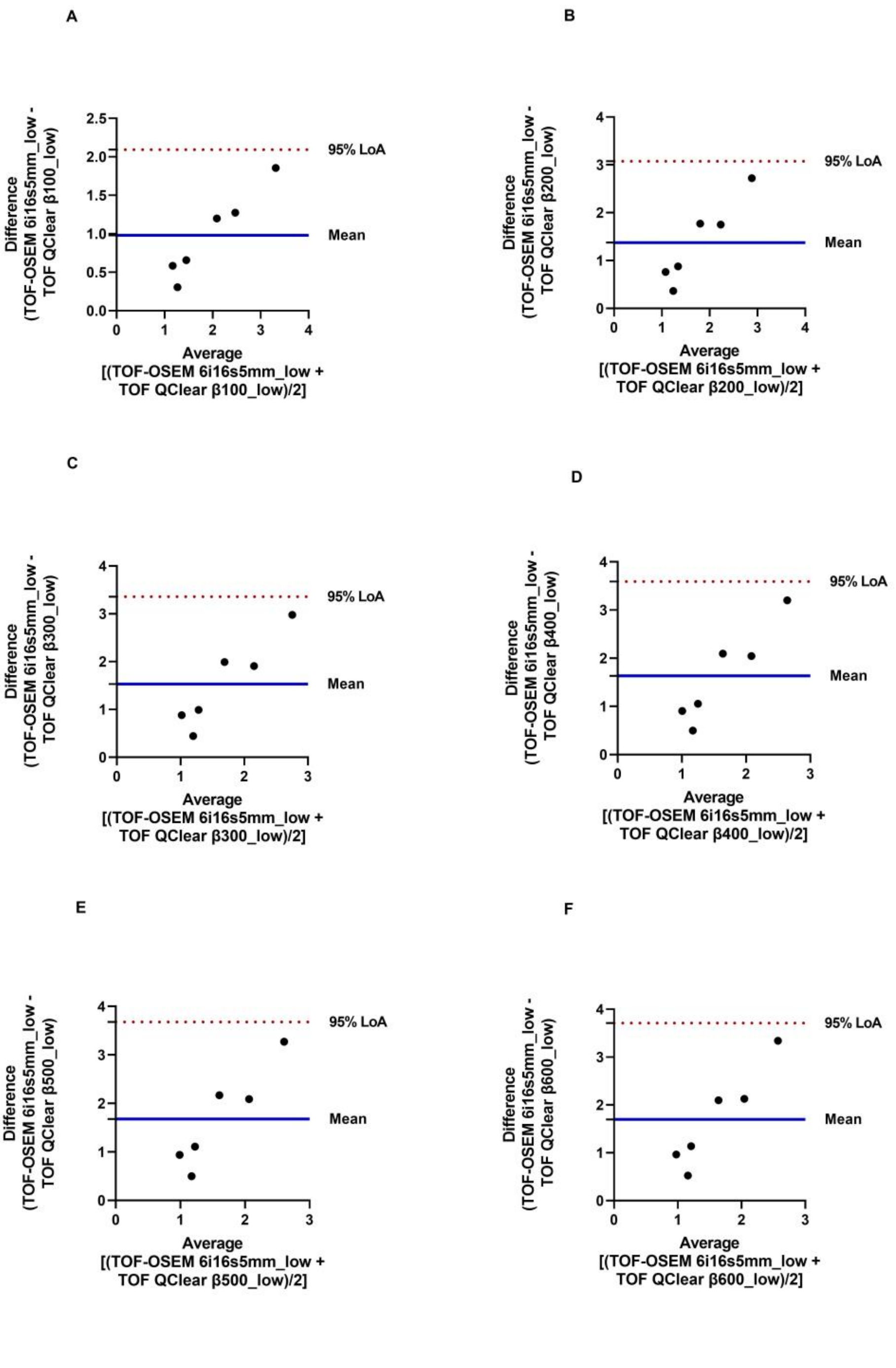

LoA = Limits of Agreement

Fig. 1 Bland-Altman plots of the BP_{ND} obtained for the Substantia Nigra: **(A)** - TOF_OSEM 6i16s5mm_low vs TOF_Q.Clear β100_low; **(B)** - TOF_OSEM 6i16s5mm _low vs TOF_Q.Clear β200_low; **(C)** - TOF_OSEM 6i16s5mm_low vs TOF_Q.Clear β300_low; **(D)** - TOF_OSEM 6i16s5mm _low vs TOF_Q.Clear β400_low; **(E)** - TOF_OSEM 6i16s5mm_low vs TOF_Q.Clear β500_low; **(F)** - TOF_OSEM 6i16s5mm_low vs TOF_Q.Clear β600_low.

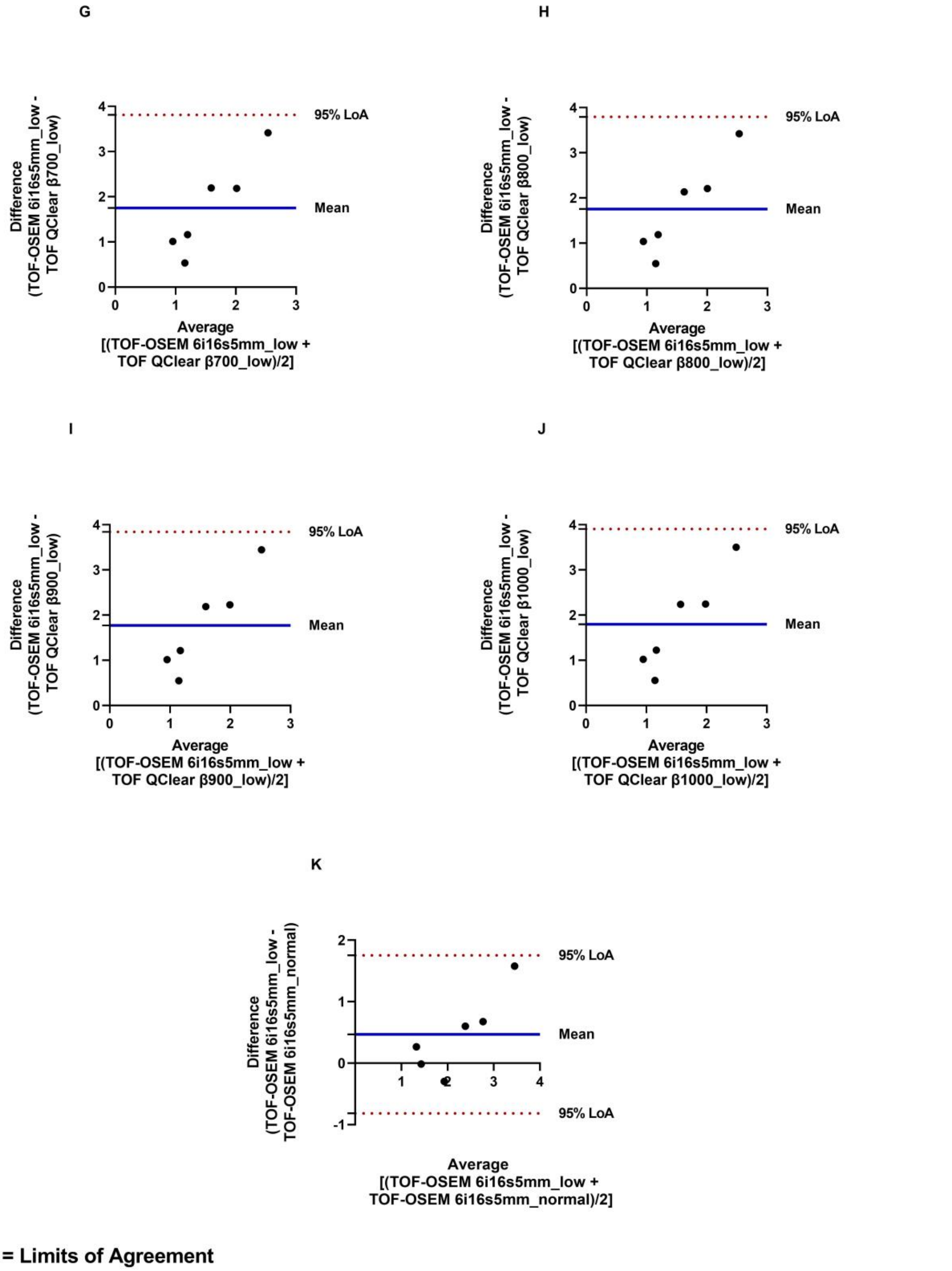

Fig. 2 Bland-Altman plots of the BP_{ND} obtained for the Substantia Nigra: **(G)** - TOF_OSEM 6i16s5mm _low vs TOF_Q.Clear β700_low; **(H)** - TOF_OSEM 6i16s5mm _low vs TOF_Q.Clear β800_low; **(I)** - TOF_OSEM 6i16s5mm_low vs TOF_Q.Clear β900_low; **(J)** - TOF_OSEM 6i16s5mm _low vs TOF_Q.Clear β1000_low; **(K)** - TOF_OSEM 6i16s5mm _low vs TOF_OSEM 6i16s5mm_normal.

Supplementary File 5

Table 1

Table 1 *Coefficient of variation obtained for the Substantia Nigra, Striatum, Globus Pallidus, Thalamus, Caudate and Putamen, per reconstruction Method. Note the highest percentages are observed for the Substantia Nigra and Thalamus.*

Reconstruction Method	%CV Substantia Nigra	%CV Striatum	%CV Globus Pallidus	%CV Thalamus	%CV Caudate	%CV Putamen
1_ TOF _OSEM_6i16s5mm_low	45.41832493	11.72287022	17.1263507	19.75959975	14.93303633	11.65408554
2_ TOF _QClear_B100_low	38.17577226	12.84491396	17.89216232	14.17978715	15.58405133	12.61996998
3_ TOF _QClear_B200_low	28.72130884	12.75007419	17.45920353	25.74974894	16.46186062	12.69296747
4_ TOF _QClear_B300_low	30.28512922	12.33280212	16.05931007	30.63244265	15.28267088	12.15481101
5_ TOF _QClear_B400_low	27.32815403	12.97046284	16.59931675	26.94987759	17.09950166	12.68228813
6_ TOF _QClear_B500_low	29.60766734	13.00523057	16.30889312	31.5792602	17.01502152	12.77713343
7_ TOF _QClear_B600_low	26.63014208	13.21577293	15.45279731	31.18768195	16.95801749	12.91191471
8_ TOF _QClear_B700_low	29.61208195	13.36629606	16.21458635	31.22143308	17.23967698	13.14849772
9_ TOF _QClear_B800_low	28.54199913	13.13942075	15.27243218	32.27131464	15.55622549	12.80121683
10_ TOF _QClear_B900_low	29.02665991	13.15239998	15.75640103	33.87790044	16.49121518	13.07511373
11_ TOF _QClear_B1000_low	30.17244768	13.45800577	16.1175274	34.42014471	18.24451088	13.31993369
12_ TOF _OSEM_6i16s5mm_normal	28.61458868	11.49902568	17.99716144	20.76490227	14.57108139	11.84132012